Proceedings of the European Conference "Physics of Magnetism" (PM'08), Poznań 2008

Structure and Magnetic Properties of Fe(Mn)–Si–B–Nb–Cu Alloys

S. Michalik[a,*], P. Sovak[a], J. Bednarcik[b], P. Kollar[a] and V. Girman[a]

[a]Department of Physics, P.J. Safarik University

Park Angelinum 9, 041 54 Kosice, Slovakia

[b]HASYLAB am DESY, Notkestr. 85, D-22603 Hamburg, Germany

According to high energy X-ray diffraction measurements no significant changes were observed in a short range atomic order of amorphous ribbons $Fe_{73.5-x}Mn_xCu_1Nb_3Si_{13.5}B_9$ ($x = 1$ up to 15 at.%). Thermal stability of the as-prepared alloys was investigated by differential scanning calorimetry and by *in situ* X-ray diffraction measurements. The two-step crystallization process was revealed, crystallization temperatures T_{x1} and T_{x2} were influenced by Mn content (thermal separation between T_{x1} and T_{x2} completely vanished for $x = 9$). Nanocrystalline state of annealed samples was confirmed by electron transmission microscopy. The influence of Mn substitution on magnetic properties was confirmed by thermomagnetic measurements.

PACS numbers: 61.05.cp, 75.50.Tt, 77.80.Bh

1. Introduction

In 1988 nanocrystalline Fe–Si–B–Nb–Cu alloys named FINEMET were patented by Yoshizawa et al. [1]. Up to this day many modifications of FINEMET have been investigated with the aim to study the influence of different elements on its crystallization processes and soft magnetic properties [2–4]. In this work authors investigate the crystallization kinetics and magnetic properties of initially amorphous Fe(Mn)–Si–B–Nb–Cu precursor and identify the role of the partial iron substitution by manganese.

2. Experimental

Amorphous ribbons approximately 2 mm wide and 30 μm thick with nominal composition $Fe_{73.5-x}Mn_xCu_1Nb_3Si_{13.5}B_9$ ($x = 1, 3, 5, \ldots$ and 15) were prepared by single-roller melt spinning technique.

Thermal responses of samples were carried out by a NETZSCH STA 409 PC/PG differential scanning calorimeter at a heating rate of 20 K/min under a continuous nitrogen flow.

The glassy structure of as-quenched samples was investigated by high energy X-rays (100 keV, wavelength 0.12398 Å) in order to get higher magnitude of wave vector transfer Q necessary for calculation of atomic pair distribution functions $g(r)$. Measurements were performed at HASYLAB at BW5 wiggler beamline.

The structural evolution during non-isothermal heating was investigated by *in situ* X-ray diffraction (XRD) (wavelength 0.493 Å) at the B2 bending magnet beamline. The annealing was performed in the temperature range of 723–1073 K with 25 K step using STOE furnace.

Nanocrystalline character of the samples annealed at 823 K for one hour was detected by transmission electron microscopy (TEM) operating at 200 keV.

The coercivity of samples annealed gradually for one hour at different temperatures was determined from hysteresis loops measured by a DC fluxmeter. The dependence of the magnetic moment on the temperature (thermomagnetic curves) was measured in the constant magnetic field 300 mT in the temperature range 300–1073 K by vibrating sample magnetometer.

3. Results and discussion

Figure 1 shows the differential scanning calorimetry (DSC) curves of samples with $x = 1, 5, 9$ and 15. It can be seen significant influence of Mn substitution on a crystallization process which evidently changes itself from the two-step process for $x < 9$ to the one-step one for $x \geq 9$. Increasing Mn content shifts onset of the first crystallization process to higher temperature T_{x1} and, on the other hand, onset T_{x2} of the second crystallization process decreases (see Table I).

The local atomic structure at the distance r from an average atom located at the origin is possible to investigate by means of a pair distribution function $g(r)$. The pair distribution function is connected with a structural factor $S(Q)$ by a Fourier transformation

$$g(r) = 1 + \frac{1}{2\pi r \rho_0} \int_0^\infty Q[S(Q) - 1] \sin(rQ)\, \mathrm{d}Q\,, \quad (1)$$

where ρ_0 is an average atomic density. The total structural factor $S(Q)$ is obtained from an elastic scattering intensity $I(Q)$ by applying the Faber–Ziman formula [5].

* corresponding author; e-mail: stefan.michalik@upjs.sk

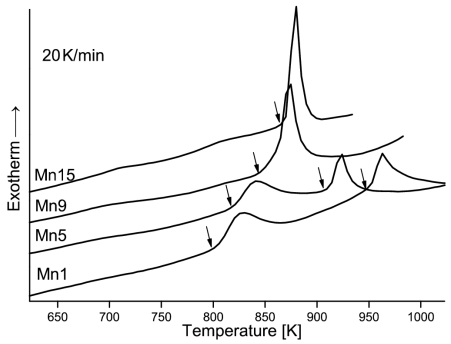

Fig. 1. DSC curves of amorphous alloys $Fe_{73.5-x}Mn_xCu_1Nb_3Si_{13.5}B_9$. Arrows mark onsets of crystallization.

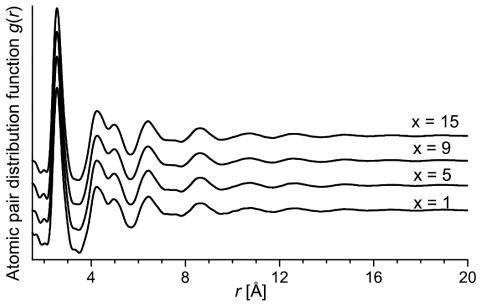

Fig. 2. Atomic pair distribution functions $g(r)$ as--quenched samples.

In Fig. 2 the atomic pair distribution functions of samples with different Mn content are displayed. In all cases $g(r)$ is characterized by one dominant peak with position at ≈ 2.55 Å followed by oscillations persisted up to 19 Å. The described character of $g(r)$ is typical of an amorphous structure and proves fully glassy state of all as-quenched samples. Changes in peak positions, periodicity of oscillations and their magnitudes depending on Mn content of as-prepared specimens are not statistically considerable. Therefore, it can be said that Mn atoms substitute Fe atoms on their original positions without any additional structural rearrangement in a short or middle range. It is consistent with the fact that Goldschmidt atomic radii [6] of Fe (1.241 Å) and Mn (1.24 Å) are practically the same. Furthermore, it is possible to analyze in more detail the first $g(r)$ peak. The first $g(r)$ peak represents contributions from all atomic pairs situated at the closest (first) coordination shell around an average atom. Those results will be published in the later work.

TABLE I

T_{x1} and T_{x2} of $Fe_{73.5-x}Mn_xCu_1Nb_3Si_{13.5}B_9$ as--quenched alloys obtained from *in situ* XRD and DSC measurements.

x [%]	T_{x1} [K]		T_{x2} [K]	
	XRD	DSC	XRD	DSC
1	798	803	948	951
5	823	818	898	907
9	848	847	873	847
15	873	869	873	869

In Fig. 3 diffraction patterns of samples with $x = 1, 5, 9$ and 15 are recorded at different stages of devitrification. At the left XRD patterns of as-quenched samples heated up to 773 K are displayed. All of them have a broad diffuse character (typical of metallic glasses) with one dominant and one less pronounced maximum followed by a shoulder at high Q side. XRD patterns for $x = 1$ and $x = 5$ samples heated up to 823 K (in the center) documents appearance of the Bragg reflection indexed as $Im3m$ Fe_3Si phase (marked by asterisk). Process of nanocrystallization has started. On the other hand, samples with $x \geq 9$ show amorphous like patterns, similar to the as-quenched stage. At the right (XRD patterns at 873 K) XRD profiles of $x = 1$ and 5 samples are without any qualitative changes compared with their previous stage. This is not more true for specimen with $x = 9$ and 15, in where the Bragg peaks appeared. XRD patterns of these samples have not only peaks belonging

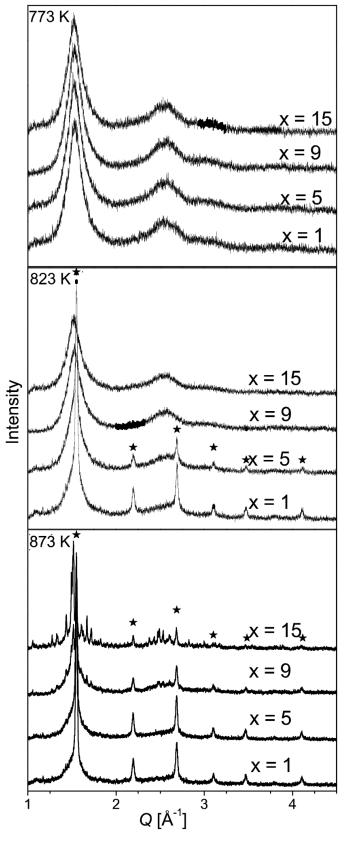

Fig. 3. XRD patterns of $Fe_{73.5-x}Mn_xCu_1Nb_3Si_{13.5}B_9$ ($x = 1, 5, 9, 15$) amorphous alloys recorded at temperatures 773 K, 823 K and 873 K. Asterisks mark $Im3m$ Fe_3Si phase.

to Fe_3Si phase but additional peaks prove a presence of other phases-borides.Temperatures T_{x1} and T_{x2} (temperatures in which first new Bragg peaks appeared) obtained from *in situ* XRD experiments are summarized and compared with results obtained from DSC in Table I. Very good coincidence can be seen between these both methods.

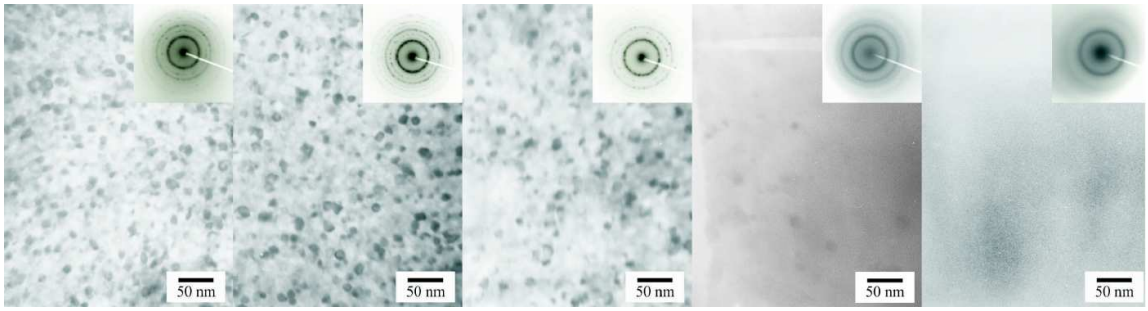

Fig. 4. Micrographs together with diffractograms of $Fe_{73.5-x}Mn_xCu_1Nb_3Si_{13.5}B_9$ with $x = 1, 3, 5, 9$ and 15 (from the left to the right) alloys annealed at 823 K.

TABLE II

T_c, T_{x1} and T_{x2} of as-quenched alloys $Fe_{73.5-x}Mn_xCu_1Nb_3Si_{13.5}B_9$ obtained from thermomagnetic curves.

x [%]	T_c [K]	T_{x1} [K]	T_{x2} [K]
1	585	798	956
3	540	808	941
5	494	814	916
7	452	827	900

Micrographs of as-quenched samples ($x = 1, 3, 5, 9, 15$) annealed at 823 K displayed in Fig. 4 document the influence of Mn substitution on the process of nanocrystallization. It can be seen that the increasing Mn content suppresses formation of a nanocrystalline phase. The sample with $x = 15$ is fully amorphous without any indication of nanocrystallites. These results are in accordance with above results from DSC and *in situ* XRD measurements. In the upper right corner of all micrographs there are shown corresponding diffractograms.

Figure 5 shows thermomagnetic curves of selected specimens ($x = 1, 3, 5, 7$). Higher Mn content causes decrease in a magnetic moment in agreement with the fact regarding antiferromagnetic character of Mn atoms compared with ferromagnetic Fe atoms. With increasing temperature the magnetic moment of all samples sharply goes down to zero value, amorphous matrix is transformed from the ferromagnetic to the paramagnetic state. Maxima of the magnetic moment are formed (see inset in Fig. 5) about 850 K and 940 K, respectively, and they indicate the formation of a ferromagnetic phase during devitrification. According to our previous results

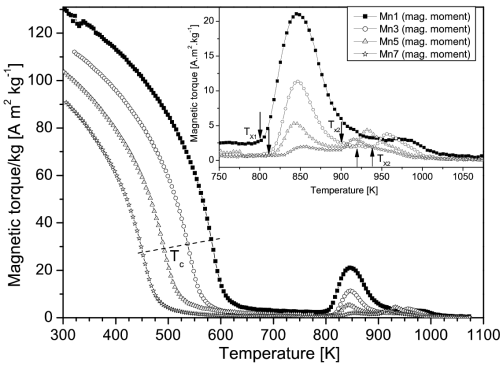

Fig. 5. Thermomagnetic curves of amorphous alloys $Fe_{73.5-x}Mn_xCu_1Nb_3Si_{13.5}B_9$. Inset shows their details in the temperature region of 750–1050 K.

the first maximum belongs to the crystallization of Fe_3Si phase and the second one could be explained as a results of borides' formation. The Curie temperature T_c of the amorphous matrix was determined from the inflection point of thermomagnetic curves. Crystallization temperatures T_{x1} and T_{x2} were estimated as the onset of maxima and together with T_c they are listed in Table II.

Measurements of hysteresis loops did not prove any noteworthy dependence of a coercivity on the Mn concentration. Initial values of coercivity for as-quenched samples with $x = 0, 1, 3, 5, 7$ were about 4.1 up to 4.8 A/m and they slightly increased in process of annealing up to 7–8 A/m at 773 K.

4. Conclusion

The aim of the work was to identify the role of the partial iron substitution by manganese in initially amor-

phous Fe(Mn)–Si–B–Nb–Cu precursors. High energy XRD measurements enabled us to calculate atomic pair distribution functions. Analysis of $g(r)$s confirmed that no considerable changes were caused by Mn substitution in the short and middle range order. Both, DSC and *in situ* XRD measurements revealed that T_{x1} increased with higher Mn content whereas T_{x2} showed an opposite tendency. Thus the temperature separation of the two crystallization events decreased with increasing Mn doping and completely vanished for 9% Mn content. Additionally, TEM confirmed the same Mn impact on the suppression of the process of nanocrystallization. Thermomagnetic measurements documented the decrement of the magnetic moment and T_c with increasing Mn content. On the other hand, the coercivity did not change significantly with changes of Mn content.

Acknowledgments

HASYLAB is gratefully acknowledged for the support during synchrotron beam time. Paper was supported by Slovak Grant Agency for Science (VEGA) grants 1/4009/07.

References

[1] Y. Yoshizawa, S. Oguma, K. Yamauchi, *J. Appl. Phys.* **64**, 6044 (1988).

[2] T. Szumiata, B Gorka, A. Zorkovska, P. Sovak, *J. Magn. Magn. Mater.* **295**, 37 (2005).

[3] G. Pavlik, P. Sovak, *J. Magn. Magn. Mater.* **304**, e678 (2006).

[4] P. Kollar, J. Kovac, J. Fuzer, E. Pancurakova, P. Sovak, M. Konc, *J. Magn. Magn. Mater.* **215-216**, 560 (2000).

[5] T.E. Faber, J.M. Ziman, *Philos. Mag.* **11**, 153 (1965).

[6] E.A. Brandes, *Smithells Metals Reference*, 6th ed., Butterworth Publ., Stoneham, MA 1983.